http://dx.doi.org/10.1109/LRA.2021.3105996

Adaptive CPG-based Gait Planning with Learning-based Torque Estimation and Control for Exoskeletons

Mojtaba Sharifi, *Member, IEEE*, Javad K. Mehr, *Student Member, IEEE*, Vivian K. Mushahwar, *Member, IEEE*, Mahdi Tavakoli, *Senior Member, IEEE*

***Abstract*—In this paper, a new adaptable gait trajectory shaping method is proposed for lower-limb exoskeletons by defining central pattern generators (CPGs). These CPGs are synchronized across different joints and updated online in response to the human users' physical behavior to enhance their safety and comfort. In this CPG structure of a high-level control scheme, an overall locomotion frequency is defined for all joint motions that can be modulated as a function of the human-robot interaction (HRI) energy. The amplitude and equilibrium position of oscillation for each joint can be adjusted in real-time based on the HRI torque. Logarithmic barrier functions are also formulated for these connected CPGs to avoid exceeding safe bounds of the joints' motion. A supervised learning algorithm is employed to identify the exoskeleton-limb dynamics and estimate the active HRI torque on different joints based on an autoregressive network with exogenous inputs (NARX) model. In order to track the reference trajectories generated by CPGs, a proportional derivative (PD) controller with torque compensation is designed. In the experimental evaluation of this intelligent control strategy, an able-bodied person wearing the Indego exoskeleton could amend and personalize the gait features considerably over a short period of time by applying active torques on different joints. In these experiments, the user increased the motion amplitude of the hip and knee joints up to 14% and made more than 200% variation in the gait frequency, which implies a considerable level of flexibility in locomotion planning for further user studies.**

***Index Terms*—Locomotion control, central pattern generator (CPG), supervised learning, NARX model, lower-limb exoskeleton, autonomous human-robot interaction**

I. Introduction

Globally, millions of people have experienced stroke, spinal cord injury, multiple sclerosis, and cerebral palsy resulting in physical impairments [1]. To improve their quality of life, assistive robotic systems are developed to help these individuals in routine activities as well as during therapy programs. In this regard, powered lower-limb exoskeletons (such as Indego [2], ReWalk [3], HAL [4], Ekso GT [5], and Exo-H3 [6]) have been invented to assist and rehabilitate individuals with neurological impairments [7]. Despite all of the endeavours in designing and deploying these systems for medical purposes, compliant interaction between the robot and wearer is an important safety issue that still needs to be addressed [8]. In order to facilitate complaint and safe human-robot interaction (HRI), autonomous strategies are required to be investigated for generating motion trajectories; however, most commercial exoskeletons have been programmed to track pre-recorded trajectories to ensure repeatability and controllability of the movements. These robotic systems have been controlled using various methods to conduct reproducible physical therapies and rehabilitation exercises [9], [10], [11], [12], in addition to performing safe interactions in assistive and resistive tasks [13], [14], [15], [16], [17].

Among the strategies suggested for motion planning of lower-limb exoskeletons and bio-inspired robots, the central pattern generator (CPG) is an appropriate one because of its inherent feature of producing time-continuous rhythmic motions synchronized for adjacent joints similar to natural bipedal locomotion. CPGs are structured as connected modules that are able to generate oscillatory movements with organized patterns in response to non-periodic inputs [18]. The functional capability of CPGs in generating fluctuating activities has been studied for the trajectory shaping of lower-limb exoskeletons in previous research studies [19]–[22]. The CPG parameters were optimized by a genetic algorithm in [19] for steady-state locomotion with a lower-limb exoskeleton implemented by a torque controller, where the knee stiffness was adjusted by activating stiffening CPG units. Gui et al. [20] benefited from CPGs and admittance control to provide flexibility in terms of the measured electromyography (EMG) signals while tracking pre-specified motion trajectories for the knee and hip joints. A robotic rehabilitation system was developed by incorporating functional electrical stimulation (FES) and torque control for a knee exoskeleton [21], where CPGs generated fixed rhythmic movements for both the FES feedforward controller and the feedback torque controller. Due to the tight coupling between the wearer and exoskeleton, it is essential to take HRI signals into account for CPG-based motion planning, which has not

Manuscript received October 15, 2020; Revised: May 31, 2021; Accepted: August 1, 2021. This paper was recommended for publication by Editor Pietro Valdastri upon evaluation of the Associate Editor and Reviewers' comments. This work was supported by the Natural Sciences and Engineering Research Council (NSERC), Canadian Institutes of Health Research (CIHR), Canada Foundation for Innovation (CFI), and the Alberta Jobs, Economy and Innovation Ministry's Major Initiatives Fund to the Center for Autonomous Systems in Strengthening Future Communities. *(Corresponding author: Mojtaba Sharifi)*

Mojtaba Sharifi, Javad K. Mehr, and Mahdi Tavakoli are with the Department of Electrical and Computer Engineering, and Sensory Motor Adaptive Rehabilitation Technology (SMART) Network, University of Alberta, Edmonton, Alberta, Canada. (e-mail: M.Sharifi@ualberta.ca, J.Khodaeimehr@ualberta.ca, Mahdi.Tavakoli@ualberta.ca)

Mojtaba Sharifi, Javad K. Mehr, and Vivian K. Mushahwar are with the Department of Medicine, and Sensory Motor Adaptive Rehabilitation Technology (SMART) Network, University of Alberta, Edmonton, Alberta, Canada. (e-mail: Vivian.Mushahwar@ualberta.ca)

Digital Object Identifier (DOI): see top of this page.

been addressed in most of previously proposed high-level control strategies.

Obtaining the interaction torque between the human and exoskeleton is a pivotal point and also a practical challenge to design appropriate control policies that are responsive to human physical behavior to enhance safety and compliance. For this purpose, EMG signals of muscles have been utilized to estimate the HRI torque [23]; however, these data suffer from significant imprecision because of electrode positioning, muscle fatigue, and skin conductivity change. Accurate force/torque sensors have also been used as an alternative sensory apparatus [24]; however, their cost and challenges in embedding them between the human limbs and exoskeleton are undeniable. In this regard, neural networks (NNs) have been employed for torque estimation, dynamic identification, trajectory shaping, and gait phase estimation for lower-limb exoskeletons. This is due to the fast rate of training and the model-free aspect of learning using NN structures, which make them desirable options for distinguishing the underlying relations between various input and output data.

An individualized motion planning was developed in [25] based on NNs in which body parameters and target walking speed were fed to a Gaussian process regression to identify and classify gait characteristics [25]. Two radial basis function neural networks (RBFNNs) were suggested to approximate passive and active HRI torques in [23]. In this work, a passive torque model was presented and EMG signals were employed for training the RBFNNs to estimate the active human torque [23]. Kang et al. [26] proposed an NN-based strategy to estimate the locomotion phase based on the hip joint angle and thigh inertial measurement unit (IMU) data as the inputs and the heel contact information as the output for offline training of the NN [26]. In a similar approach, a nonlinear autoregressive network with exogenous inputs (NARX) was utilized to capture the ankle joint dynamics based on the collected data of a typical walking [27]. The EMG activity of shank muscles and knee joint position were considered the inputs, and the ankle joint position as the NARX structure's output to be estimated [27]. In another study, NARX was employed in the estimation of the foot angular position for the purpose of controlling an active prosthetic [28]. The gait data from seven able-bodied people were used in the training process and the angular volocity of the shank was considered as the input of the network [28].

In the present study, an intelligent strategy is presented based on a new CPG structure for modulating and controlling of a lower-limb exoskeleton that results in a compliant and safe physical interaction with the human. The proposed CPG dynamics has adaptable online features to update the gait characteristics in response to the HRI. In order to estimate HRI torque and energy transmitted through different joints, a multi-layer NN with the NARX model is utilized as a learning algorithm. To this end, the neural network is trained first in a supervised fashion to estimate the closed-loop nonlinear dynamics of the multi-DOF exoskeleton-limb system with various position and velocity trajectories. The responsive features of the proposed adaptable CPGs that enable the wearers to accelerate/decelerate, magnify and shift the synchronized motions of all exoskeleton joints for the bipedal locomotion can be summarized as follows.

- The overall gait frequency is tunable in real-time in terms of the HRI energy transmitted through all exoskeleton joints.
- The oscillation range for each joint trajectory is also adjustable online based on the HRI energy, while its initial trend is determined by a Fourier series analysis on experimental sample gait data.
- The mean value of each joint's motion as its equilibrium position is regulated for each person in response to the time integral of HRI torque.

Subtracting the learned passive dynamics from the simultaneous joint torque during the main gait cycle, the active HRI torque is determined. Having a PD controller combined with the HRI torque compensation, an appropriate tracking of joint trajectories (generated by CPGs) is facilitated.

II. Adaptive CPG-Based Gait Planning

The nonlinear dynamics of a multi-DOF lower-limb exoskeleton interacting with the human user is represented as

$$M_q(q)\ddot{q} + C_q(q)\dot{q} + G_q(q) - \tau_{hum_{pas}} = \tau_{mot} + \tau_{hum_{act}} \quad (1)$$

where q is the vector of exoskeleton joints' position, $M_q(q)$ is the inertia matrix, $C_q(q)$ is the matrix of Coriolis, centrifugal and damping terms, $G_q(q)$ is the vector of gravitational torques, τ_{mot} is the exoskeleton's motor torque, and $\tau_{hum_{pas}}$ and $\tau_{hum_{act}}$ are passive and active portions of the human torque vector.

Our proposed adaptable CPG is formulated for high-level control of the exoskeleton to manage both legs' locomotion trajectories in real-time. This CPG dynamics is proposed for variations of the overall locomotion frequency $\omega(t)$, equilibrium position $\xi_i(t)$ and oscillation amplitude $\rho_i(t)$ of each lower-limb joint's motion and its phase variation $\phi_i(t)$ by a nonlinear coupled system as

$$\begin{aligned}
\ddot{\omega}(t) =& \gamma_\omega\Big(\frac{\gamma_\omega}{4}\big(\Omega + \sum_{k=1}^{n}\psi_k E_k(t) - \omega(t)\big) - \dot{\omega}(t)\Big)\\
\ddot{\rho}_i(t) =& \gamma_\rho\Big(\frac{\gamma_\rho}{4}\big(A_{\rho_i} + \lambda_i E_i(t) - \rho_i(t)\big) - \dot{\rho}_i(t)\Big)\\
&+ k_\rho\, u(\rho_i(t) - \rho_{i_{th_+}}) \log\left(\frac{\rho_{i_{max}} - \rho_i(t)}{\rho_{i_{max}} - \rho_{i_{th_+}}}\right)\\
\ddot{\xi}_i(t) =& \gamma_\xi\Big(\frac{\gamma_\xi}{4}\big(A_{\xi_i} + \beta_i T_i(t) - \xi_i(t)\big) - \dot{\xi}_i(t)\Big)\\
&+ k_{\xi_1}\, u(\xi_i(t) - \xi_{i_{th_+}}) \log\left(\frac{\xi_{i_{max}} - \xi_i(t)}{\xi_{i_{max}} - \xi_{i_{th_+}}}\right)\\
&- k_{\xi_2}\, u(\xi_{i_{th_-}} - \xi_i(t)) \log\left(\frac{\xi_{i_{min}} - \xi_i(t)}{\xi_{i_{min}} - \xi_{i_{th_-}}}\right)\\
\dot{\phi}_i(t) =& \omega(t) + \sum_{j=1}^{m_i}\eta_{ij}\,\sin(\phi_i(t) - \phi_j(t) - \Delta\phi_{ij})
\end{aligned} \quad (2)$$

in which n is the number of active exoskeleton joints on the right and left legs, and m_i is the number of adjacent joints to the joint i. γ_ω, γ_ρ and γ_ξ are constant parameters.

$\rho_{i_{th_+}}$ is the positive threshold value of $\rho_i(t)$ that triggers the deceleration term with the gain k_ρ to avoid reaching the maximum allowable amplitude $\rho_{i_{max}}$ of oscillation for each joint. $\xi_{i_{th_+}}$ and $\xi_{i_{th_-}}$ are the positive and negative thresholds $\xi_i(t)$ that if exceeded the deceleration and acceleration terms with the gains k_{ξ_1} and k_{ξ_2} to not cross the maximum and minimum allowable magnitudes $\xi_{i_{max}}$ and $\xi_{i_{min}}$ for the equilibrium position of each joint. $u(.)$ is the step function that activates the $\log(.)$ function when the corresponding thresholds mentioned above are crossed. ψ_i, λ_i and β_i are constant gains for updating frequency, amplitude and equilibrium of the gait cycles, respectively, based on the injected HRI energy E_i and the time integral of corresponding HRI torque T_i, which are defined for each joint i as

$$\begin{aligned} E_i(t) &= \int_0^t \tau_{HRI_i}(t)\ \dot{q}_i(t)\ dt \\ T_i(t) &= \int_0^t \tau_{HRI_i}(t)\ dt \end{aligned} \tag{3}$$

where $\dot{q}_i(t)$ is the velocity of the exoskeleton's joint i, and $\tau_{HRI_i}(t)$ is the estimated human torque on this joint after applying a dead-zone function:

$$\tau_{HRI_i} = \begin{cases} \hat{\tau}_{hum_{act_i}} - \tau_{th_+} & \hat{\tau}_{hum_{act_i}} > \tau_{th_+} \\ 0 & \tau_{th_-} \le \hat{\tau}_{hum_{act_i}} \le \tau_{th_+} \\ \hat{\tau}_{hum_{act_i}} - \tau_{th_-} & \hat{\tau}_{hum_{act_i}} < \tau_{th_-} \end{cases} \tag{4}$$

in which τ_{th_-} and τ_{th_+} are the negative and positive thresholds of this dead-zone function. Wearers can modify the gait cycle characteristics if they apply any torque beyond these thresholds. The reference trajectory for the joint i of the exoskeleton is defined using Fourier series expansion as

$$q_{r_i}(t) = \xi_i(t) + \rho_i(t) \sum_{l=1}^{S_i} (c_{i_l} \cos(l\phi_i(t)) + d_{i_l} \sin(l\phi_i(t))) \tag{5}$$

where c_{i_l} and d_{i_l} are the coefficients of the Fourier series (with S_i terms) that initially harmonize the reference motion of the joint i with a typical walking trajectory. The equilibrium $\xi_i(t)$, amplitude $\rho_i(t)$ and phase $\phi_i(t)$ of each joint's oscillatory motion in (5) are amended in real-time by the proposed CPG-based update rules (2), as illustrated in Figs. 1(a) and 1(b). As the reference trajectory generated in (5) is time-continuous and differentiable, the proposed learning-based control strategy can facilitate a smooth tracking performance. Other features of the proposed adaptive locomotion planning (2) and (5) are mentioned as follows.

Synchronized gait trajectories are generated for different joints with the same overall frequency $\omega(t)$. The other coupling between phases of adjacent joints is defined by the $\sin(.)$ function in the connected dynamics of $\phi_i(t)$ in (2), based on the methodology proposed in [18]. The amplitude of each joint trajectory $\rho_i(t)$ is amended online based on (2), while the corresponding initial Fourier coefficients c_{i_l} and d_{i_l} are specified from the analysis of experimental data. The transmitted HRI energy $E_i(t)$ through each joint i of the exoskeleton can modify the range of oscillation $\rho_i(t)$ for that joint. The gait frequency $\omega(t)$ is also adjusted in real-time according to (2) in terms of the HRI energy $\sum_{k=1}^{n} \psi_k E_k(t)$ transmitted through all exoskeleton joints with the scaling factors of ψ_k. Due to this feature, by applying the interaction torques and transferring energy $E_i(t)$, the wearer is capable of accelerating or decelerating the synchronized locomotion speed/frequency of all n joints of the exoskeleton. If the applied HRI torque τ_{HRI_i} is in the same direction as the velocity $\dot{q}_i$ for each joint over time, the wearer will inject energy to the system based on (3) and this would increase the walking speed. Conversely, having the torque and velocity in opposite directions and making negative E_i in (3) would result in the speed reduction in (2). At the same time, human users can increase or decrease the range of motion for each joint with the authority factor of λ_i for any symmetric or asymmetric walking. In addition, a logarithmic barrier function is defined in (2) to control and decelerate the rising rate of $\rho_i(t)$ after crossing the threshold $\rho_{i_{th_+}}$ to stay below the maximum allowable amplitude $\rho_{i_{max}}$ of each joint oscillation regarding the exoskeleton's feasible range of movement.

The other variable that is adjusted in the proposed CPG-based gait planning (2), in response to the time integral of HRI torque T_i, is the equilibrium position $\xi_i(t)$ of each joint's motion. This is due to the difference in mean values of joint trajectories for various individuals with or without disabilities. However, if a human user exceeds the upper or lower threshold ($\xi_{i_{th_+}}$ or $\xi_{i_{th_-}}$) of this mean value, a logarithmic barrier function in the dynamics of $\xi_i(t)$ will be activated to decelerate its magnitude variation with the gains of k_{ξ_1} and k_{ξ_2}. These thresholds and barrier functions are devised to ensure that the maximum and minimum allowable magnitudes of equilibrium positions $\xi_{i_{max}}$ and $\xi_{i_{min}}$ are not crossed.

III. Learning-Based HRI Torque Estimation and Tracking Controller

In this section, an NN-based technique is utilized in a supervised fashion to learn the dynamics of the exoskeleton-limb system (1) and finally estimate the active HRI torque $\tau_{hum_{act}}$. To this end, the NARX neural network model is employed to learn the exoskeleton-limb dynamics and estimate HRI torque. The estimated HRI torque is employed in the proposed adaptive CPG structure to shape the gait trajectories of all joints based on the wearer's intention. At the same time, the estimated HRI is compensated in tracking control law to follow the generated reference trajectories properly, as depicted in Fig. 1(a).

A. NARX Neural Network Scheme

Since the development of NNs, they have been explored as appropriate computing systems with generalization properties that are beneficial for identifying dynamic systems and predicting their time-series responses [29]. The NARX is a dynamic recurrent network which has been widely used in the dynamic identification of different robotic systems [27], [28], [30]. This network has outstanding capabilities in effective learning including fast convergence, high accuracy, and appropriate generalization compared to the conventional recurrent neural networks [29], [30]. Also, the employment of the historical data in the estimation of the system's current output, makes the

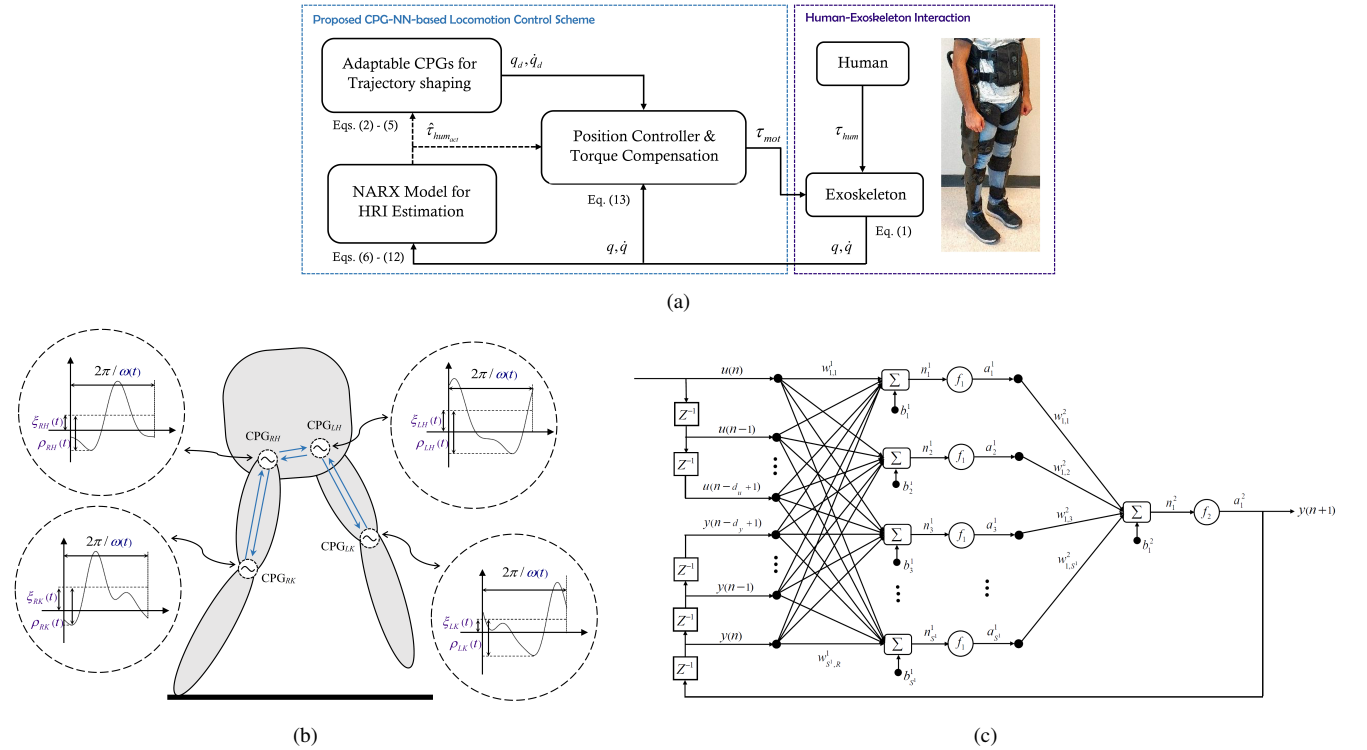

Fig. 1. Adaptive CPG-based gait planning: (a) control architecture, (b) CPG structure for online adjustment of the locomotion's frequency, amplitude and mean value, and (c) NARX model for the estimation of active HRI torque

NARX an excellent tool for the identification of nonlinear dynamics. Accordingly, the NARX structure is taken into account in this study to learn the nonlinear passive dynamics of the human-exoskeleton system (the left side of (1)). This learning is organized based on preliminary experimental data gathered when the exoskeleton is worn by the user, and the whole system is driven and moved by motors τ_{mot} with minimum active torque generation $\tau_{hum_{act}}$ (by relaxing the lower-limb muscles). Position, velocity, and torque data for all joints of the human-exoskeleton system are collected for various locomotion patterns (frequencies and amplitudes). These data are used to train and assess the NN with the joint position and velocity considered as the input $u(t)$ and the motor torques as the output $y(t)$ of this network. The discrete-time nonlinear function of the NARX model [31] is defined as

$$\begin{aligned} y(t) =& f[y(t-1), y(t-2), ..., y(t-d_y); u(t-1), \\ & u(t-2), ..., u(t-d_u)] \end{aligned} \tag{6}$$

where $u(t)$ and $y(t)$ are input and output vectors of this model, and d_y and d_u denote the input and output memory orders, respectively. A schematic of the employed NARX neural network with one hidden-layer is depicted in Fig. 1(c). Considering k as the current time step, the input of each neuron in the hidden layer at time $k+s$ is given as [32]

$$\begin{aligned} n_i^1(k+s-1) =& \ b_i^1 + \\ & \sum_{j=1}^{min(s,d_u)} w_{i,j}^1 u(k+s-j) + \sum_{j=s+1}^{d_u} w_{i,j}^1 u(k+s-j) + \\ & \sum_{j=1}^{min(s-1,d_y)} w_{i,j+d_u}^1 y(k+s-j) + \sum_{j=s}^{d_y} w_{i,j+d_u}^1 y(k+s-j) \end{aligned} \tag{7}$$

where $w_{i,j}^1$ are weights and b_i^1 are biases of this network. The outputs of the hidden layer and output layer are defined respectively as

$$\begin{aligned} n_1^2(k+s) =& \sum_{i=1}^{S^1} w_{1,i}^2 f_1 \left[n_i^1(k+s-1)\right] + b_1^2 \\ y(k+s+1) =& \ a_1^2(k+s+1) = \ f_2 \left[n_1^2(k+s)\right] \end{aligned} \tag{8}$$

in which S^1 denotes the number of neurons in the hidden layer. f_1 and f_2 are activation functions of hidden and output layers, set to be tangent-sigmoid and purelin functions, respectively.

Two different modes of the NARX neural network were suggested in the literature, including the parallel and series-parallel modes [27]–[30]. The estimated output is fed back to the neural network's inputs in the parallel mode; however, the real values of output are used in the series-parallel mode [31]. In this study, the series-parallel mode is utilized to avoid error accumulation and achieve a more accurate HRI torque estimation.

B. Learning Algorithm

Having m samples from one set of data, the mean square error (MSE) and the cost function (J) are formulated as [32]

$$\begin{aligned} MSE(w,b) =& \frac{1}{m} \sum_{k=1}^{m} [y(k) - \hat{y}(k)]^2 \\ J(w,b) =& MSE(w,b) + \frac{1}{m} \lambda \sum_{w} w^T w \end{aligned} \tag{9}$$

where w and b are the weight and bias values in the NARX structure, and $\lambda > 0$ is the regulation parameter. In order to determine the minimum amount of the cost function (J), the

partial derivatives of that with respect to w and b need to be minimized. The steepest descent method is used for this purpose, which results in the following update rule for the structural NARX parameters for each iteration [32]

$$\begin{aligned} b_{next} &= b_{current} - \alpha \frac{\partial}{\partial b}(MSE) \\ w_{next} &= (1 - \frac{\alpha\lambda}{m}) w_{current} - \alpha \frac{\partial}{\partial w}(MSE) \end{aligned} \tag{10}$$

in which α is the learning rate of the steepest descent method. Note that the output of this learning technique is the estimated dynamics of the combined exoskeleton-limb system (the left side of (1)) for each joint i with minimum active torque $\tau_{hum_{act}}$ obtained from preliminary experiments:

$$\hat{\tau}_{dyn_i}(t) = y(t) \tag{11}$$

Given this estimation, the active HRI torque can be estimated in the main experiments based on (1) at any instance of the motion as

$$\hat{\tau}_{hum_{act_i}}(t) = \tau_{mot_i}(t) - \hat{\tau}_{dyn_i}(t) \tag{12}$$

which is employed in the proposed adaptive CPG structure (2)-(4).

C. Tracking Controller with Torque Compensation

As a result of learning the exoskeleton-limb dynamics in various positions and velocities using the NARX model and estimating $\tau_{hum_{act}}$, this torque can be compensated in the control law to achieve a precise trajectory tracking performance. Accordingly, the position controller is designed as a combination of an error-based proportional derivative (PD) term and a torque compensation term as the output of proposed learning-based torque estimation:

$$\tau_{mot_i}(t) = K_p(q_{r_i}(t) - q_i(t)) + K_d(\dot{q}_{r_i}(t) - \dot{q}_i(t)) + \hat{\tau}_{hum_{act_i}}(t) \tag{13}$$

where K_p and K_d are the constant gains of this tracking controller. Note that a typical PD controller, without any torque estimation/compensation or having any online trajectory shaping, is embedded in the Indego exoskeleton system (the testbed in this work) for clinical gait therapy.

IV. Experimental Evaluations

The proposed autonomous control strategy was assessed experimentally to evaluate its adaptive capabilities in gait trajectory planning and control using the Indego exoskeleton (Parker Hannifin Corporation). An able-bodied user (27-year-old male) wore the exoskeleton and used a safety harness connected to an overhead lift to avoid injury in the event of falling, as shown in Fig. 2. This experiment was planned to demonstrate the adaptiveness of locomotion trajectories in response to different arbitrary HRI torques on different joints of the exoskeleton. MATLAB-Simulink was employed in the real-time mode as the control software to implement the proposed strategy, receiving the sensory data and sending the command to actuators at a sampling rate of 200 Hz. Using a CAN interface (Vector VN1610) with 2 channels, the exoskeleton was connected to the operating system (a Core i7 laptop with 16GB RAM) via USB to implement the control

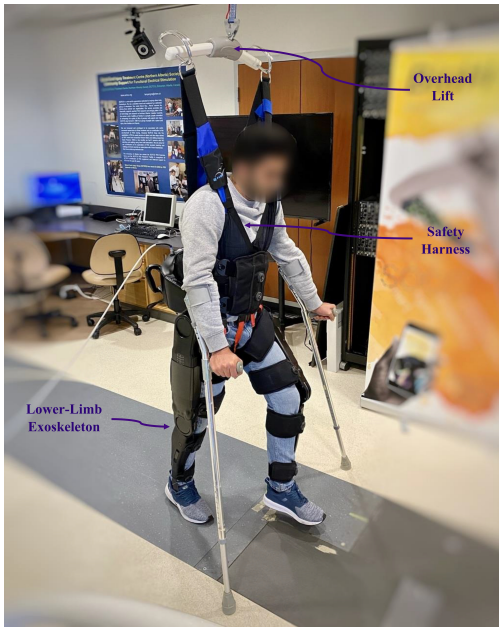

Fig. 2. Indego lower-limb exoskeleton assisting a human user in overground walking with a safety harness

strategy. Preliminary tests were first carried out to learn the passive human-exoskeleton dynamics using the NARX model (presented in Sec. III-A), which were required to estimate the active HRI torque in the proposed strategy.

A Fourier analysis was carried out on the primary hip and knee motions captured from a typical human gait motion [33], in which eight terms of this series ($S_i = 8$ in (5)) were sufficient to estimate trajectories accurately. The coefficients of these terms are listed in the Appendix. The bipedal phase difference between the left and right legs' motions is π rad. Initial values and parameters of the proposed CPG scheme for the hip and knee joints are provided in the Appendix. These values were specified by trial-and-error, and performing initial tests to achieve user comfort as well as smooth variation of the locomotion trajectory by applying interaction torques around different joints. Accordingly, the exoskeleton flexibility was assessed to display enough deviation from the primary trajectory based on the human interaction by appropriate regulation of CPG gains. In this trial-and-error method, increasing the gains ψ_i, λ_i and β_i in (2) increased the human authority in modifying gait speed, and amplitude and equilibrium position of each joint. Moreover, by decreasing the gains γ_ω, γ_ρ and γ_ξ, the response of trajectory variation became smoother (with smaller accelerations) and more damped. Ω in (2) is the predetermined frequency of walking chosen by the user before online modification. $\rho_{i_{th_+}} = 1.1 - 1.15$ and $\rho_{i_{max}} = 1.2$ were regulated in (2) to avoid exceeding the joint limits of the exoskeleton during the primary trajectory of locomotion, as described in Section II. $\xi_{i_{th_+}}$ and $\xi_{i_{th_-}}$ were chosen and listed in the Appendix to have a range of 10-12 degrees of variation to amend the equilibrium positions of the hip and knee joints for each person with respect to the typical gait cycle.

Preliminary experiments were performed while the human user wore the exoskeleton and relaxed his lower extremity

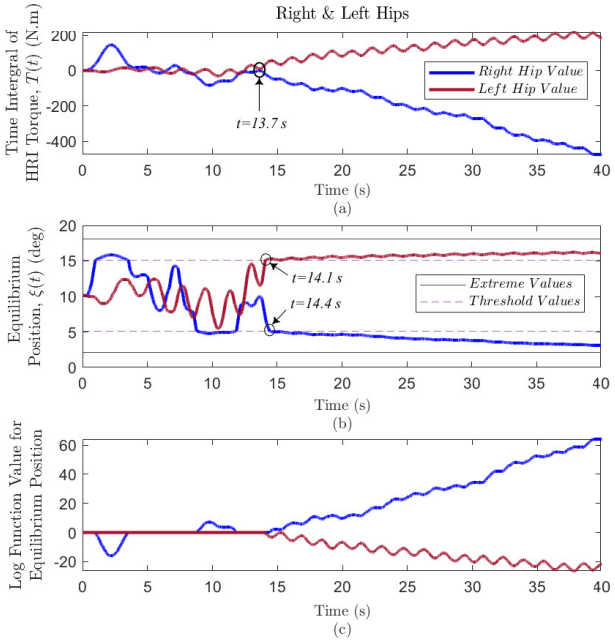

Fig. 3. Variation of (a) interaction torque integral, (b) equilibrium position, and (c) corresponding logarithmic function value for the right and left hip joints

muscles such that minimum active muscle force was generated. The motion (position and velocity) and actuation (torque) data for twenty repetitions, each for 300 seconds, were gathered and combined to include various walking scenarios. These preliminary tests were used to identify the nonlinear passive dynamics of the human-exoskeleton system, as described in Section III-A. Between these empirical tests, the amplitude of walking for different joints had a maximum of 20% variation due to the motion limit of the exoskeleton joints, and the speed of walking experienced a 200% change from the original locomotion pattern (designed to have hip and knee amplitudes of 59 and 70 degrees, and walking frequency of 1.41 rad/s). Also, the equilibrium position for each joint motion had a variation of 100% from the initial value considered at the beginning of the main experiments to cover a wide range of joint motion for human locomotion. The initial magnitudes of the gait parameters are listed in the Appendix. Seventy percent of the collected data in preliminary experiments was used for offline training of the NARX model, 15% of that was employed for assessment of the torque estimation, and 15% for validation. The NARX model was structured with ten hidden neurons and two steps of time delay. The Bayesian Regularization method was utilized for training and the maximum torque estimation error after 1 epoch of training (with less than 300 iterations) was 1.5×10^{-3} N.m, which is negligible.

After offline training of the NARX model using the obtained motion and actuation data from the passive dynamics of the human-exoskeleton system, this model was utilized in real-time by the Function Fitting Neural Network block in the Simulink environment. The passive dynamics $\hat{\tau}_{dyn_i}(t)$, approximated with high accuracy, was employed in (12) to estimate the active human torque $\hat{\tau}_{hum_{act_i}}(t)$ in the main experiments. For both preliminary and main tests, the user wore a safety harness attached to an overhead lift during walking

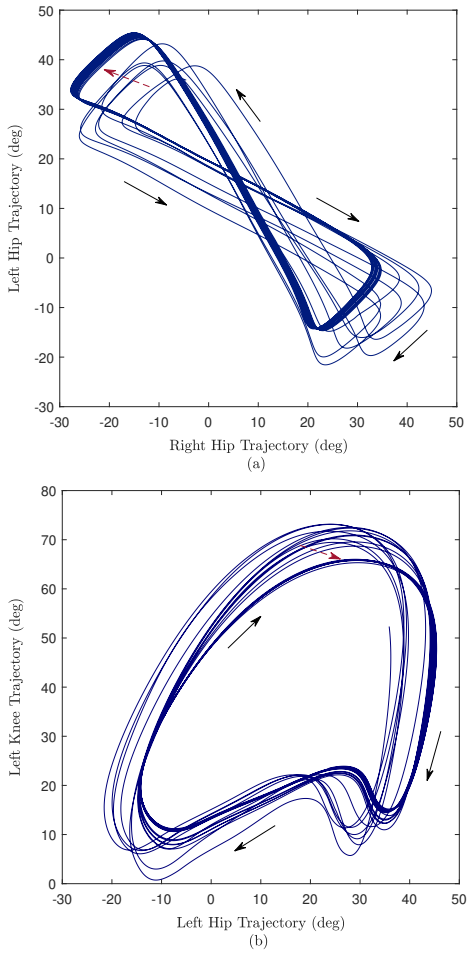

Fig. 4. Variation of trajectories for (a) left hip with respect to right hip, and (b) left knee with respect to left hip (black arrows show the direction of locomotion and red arrows show the direction of trajectory deviation)

that prevented injury in the case of falling as seen in Fig. 2. In this experiment, a human operator applied arbitrary torques on different joints to change the equilibrium position $\xi_i(t)$ of locomotion and make it personalized for user. The rapid variation of this equilibrium in response to the time integral of HRI torques $T_{Right\,Hip}$ and $T_{Left\,Hip}$ is demonstrated in Fig. 3 based on the proposed adaptive CPG dynamics (2).

As seen, the HRI torques of the right and left hips experienced variations at the beginning of walking while they became respectively negative and positive from $t = 13.7$ s, resulting in a decline of $\xi_{RightHip}(t)$ and an elevation of $\xi_{LeftHip}(t)$. Consequently, $\xi_{Right\,Hip}(t)$ passed its negative threshold value $\xi_{H_{th_-}} = 5.13$ degrees at $t = 14.4$ s and $\xi_{Left\,Hip}(t)$ exceeded its positive threshold value $\xi_{H_{th_+}} = 15.13$ degrees at $t = 14.1$ s. In response, the logarithmic barrier functions in (2) were activated and returned non-zero values to decelerate these variations and avoid the extreme magnitudes $\xi_{H_{min}} = 2.13$ degrees and $\xi_{H_{max}} = 18.13$ degrees. The logarithmic function was zero when the equilibrium position variation for each joint was within its allowable range.

To elaborate more on the autonomous shaping of the gait cycles, the reference trajectory of the left hip with respect to the right hip and left knee motions are shown in Fig. 4. The smooth modification of the mean values for the right and left hip motions is observed by the movement of its

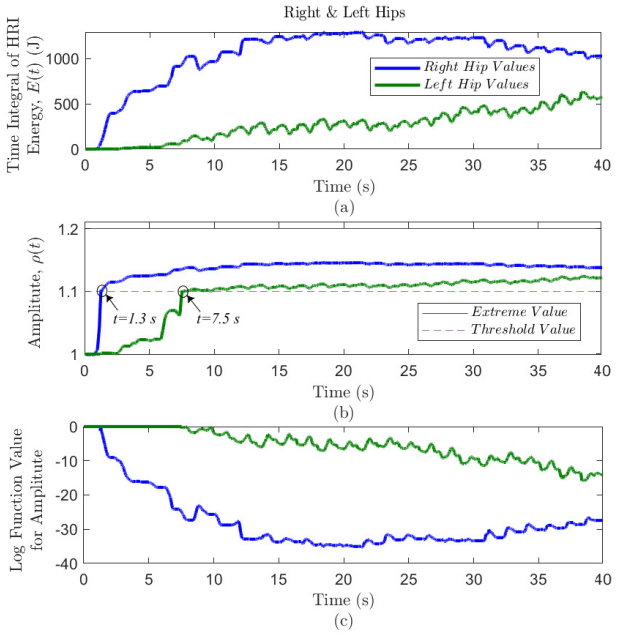

Fig. 5. Variation of (a) injected HRI energy, (b) motion amplitude, and (c) corresponding logarithmic function value for the right and left hip joints

relative trajectories. This implies a shift of the relative hip trajectories to the top and left due to the increase of the left hip's equilibrium position and the decrease of the right hip's equilibrium position, as illustrated by red arrows in Fig. 4(a). In this regard, the pattern of left hip-knee trajectories experienced a movement toward the right and bottom in Fig. 4(b).

The wearer also applied active torques on different joints of the exoskeleton to amend their oscillation ranges of motion $\rho_i(t)$ according to (2). As illustrated in Fig. 5, the increase of HRI energy transferred through the right and left hip joints $E_{Right\,Hip}$ and $E_{Left\,Hip}$ over the first stride resulted in a maximum growth of 14% and 11% in the amplitude $\rho_{Right\,Hip}(t)$ and $\rho_{Left\,Hip}(t)$ of these joints' motions. This variation exceeded the amplitude threshold $\rho_{Hip_{th_+}} = 1.1$ at $t = 1.3$ s and $t = 7.5$ s for the right and left hips, respectively, and turned the corresponding logarithmic function on to restrict this escalation. This function gained negative values over the next steps to hold the amplitudes of hip joints below their maximum feasible magnitude $\xi_{Hip_{max}} = 1.2$.

Having these adjustable features for shaping the gait cycles and considering feasible motions for exoskeleton joints, the reference trajectories were generated in real-time as demonstrated in Fig. 6(a) for the right hip and left knee. Suitable tracking performance using the proposed PD controller with torque compensation (13) was attained with small bounded errors in their steady-state response (2 and 4 degrees for the right hip and left knee, respectively). The fluctuation of the right hip equilibrium position (illustrated in Fig. 3) and the variation of the maximum value of the left knee motion are also depicted in Fig. 6(a). Regarding the speed of walking, the wearer torques on different joints could modify the overall locomotion frequency $\omega(t)$ due to its dynamics (2). As seen in Figs. 6(b) and 6(c), by transferring energy through all of the joints $E_i(t)$, the locomotion accelerated and the gait frequency increased from 1.41 rad/s to 4.08 rad/s. After this online adjustment in the first 15 s, the user continued walking with this higher speed for the rest of the path.

V. Conclusion

In this study, an intelligent control strategy was designed and tested to provide comfortable and safe bipedal locomotion using lower-limb exoskeletons. To this end, a new CPG structure was proposed to generate synchronized oscillatory motions for different joints that are responsive to the active HRI torque. This adaptiveness was facilitated by the amendment of the gait frequency, amplitudes of reference trajectories, and equilibrium positions in terms of the HRI energy and torques transmitted through the exoskeleton joints. A supervised NN-based learning algorithm was utilized based on the NARX model to learn the passive exoskeleton-limb dynamics and then estimate the active HRI torque in the joint space. This control strategy was implemented on the Indego exoskeleton (Parker Hannifin Corporation), and experimental results showed suitable flexibility for different locomotion features (with variations in amplitude, equilibrium, and frequency) in the presence of active human behavior. In this work, we gained the benefits of fast supervised learning of the HRI dynamics and online trajectory shaping by designing a new adaptive CPG structure that can adjust the gait cycles according to the wearer's intention. However, the following technical challenges and limitations should be addressed in future studies: (i) designing a nonlinear controller for trajectory tracking that facilitates close-loop stability analysis (instead of the proposed PD controller with torque compensation), and (ii) employing reinforcement learning algorithms to update the approximation of system dynamics during the main walking task considering changes or disturbances in the environment or HRI.

APPENDIX

Initial state values, threshold and extreme values, and the CPG parameters in (2), (4) and (5) for the hip (H) and knee (K) joints are provided in https://github.com/tbs-ualberta/RAL_NN_CPG_Control_Lower-limb_Exoskeleton.

References

[1] M. Sharifi et al., "Patient-Robot-Therapist Collaboration Using Resistive Impedance Controlled Tele-Robotic Systems Subjected to Time Delays," *Journal of Mechanisms and Robotics*, vol. 10, p. 061003, 2018.

[2] S. A. Murray et al., "Fes coupled with a powered exoskeleton for cooperative muscle contribution in persons with paraplegia," in *Annual International Conference of the IEEE Engineering in Medicine and Biology Society (EMBC)*, 2018, pp. 2788–2792.

[3] G. Zeilig et al., "Safety and tolerance of the rewalk™ exoskeleton suit for ambulation by people with complete spinal cord injury: a pilot study," *The Journal of Spinal Cord Medicine*, vol. 35, pp. 96–101, 2012.

[4] O. Jansen et al., "Hybrid assistive limb exoskeleton hal in the rehabilitation of chronic spinal cord injury: proof of concept; the results in 21 patients," *World neurosurgery*, vol. 110, pp. 73–78, 2018.

[5] R. W. Evans et al., "Robotic locomotor training leads to cardiovascular changes in individuals with incomplete spinal cord injury over a 24-week rehabilitation period: a randomized controlled pilot study," *Archives of Physical Medicine and Rehabilitation*, 2021.

[6] K. A. Inkol and J. McPhee, "Assessing control of fixed-support balance recovery in wearable lower-limb exoskeletons using multibody dynamic modelling," in *8th IEEE RAS/EMBS International Conference for Biomedical Robotics and Biomechatronics (BioRob)*, pp. 54–60.

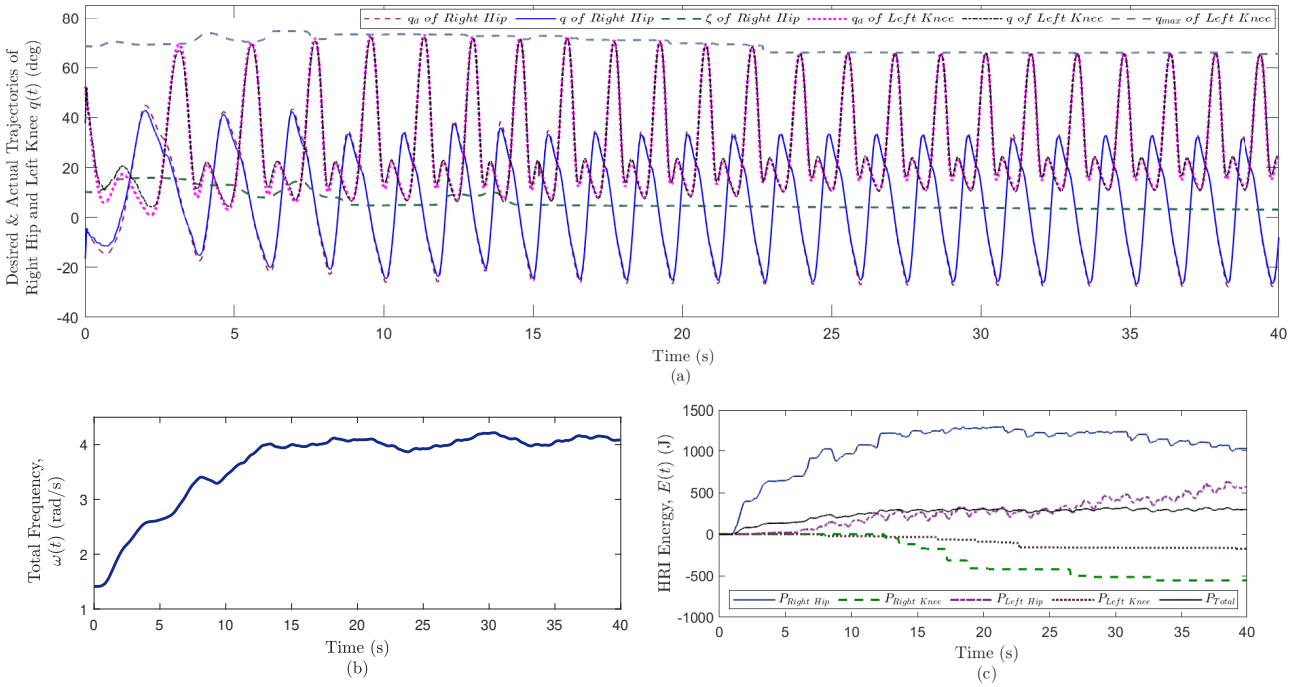

Fig. 6. Amendment of (a) response trajectories with adjustment of equilibrium position and amplitude of the motion for the right hip and left knee, (b) overall locomotion frequency, and (c) HRI energy transferred through all joints

[7] A. Esquenazi et al., "Powered exoskeletons for walking assistance in persons with central nervous system injuries: a narrative review," *PM&R*, vol. 9, no. 1, pp. 46–62, 2017.

[8] V. Azimi et al., "Robust ground reaction force estimation and control of lower-limb prostheses: Theory and simulation," *IEEE Transactions on Systems, Man, and Cybernetics: Systems*, vol. 50, pp. 3024–3035, 2020.

[9] A. A. Blank et al., "Current trends in robot-assisted upper-limb stroke rehabilitation: Promoting patient engagement in therapy," *Current Physical Medicine and Rehabilitation Reports*, vol. 2, p. 184–195, 2014.

[10] M. Sharifi et al., "Impedance variation and learning strategies in human-robot interaction," *IEEE Transactions on Cybernetics*, pp. 1–14, 2021.

[11] W. Meng et al., "Recent development of mechanisms and control strategies for robot-assisted lower limb rehabilitation," *Mechatronics*, vol. 31, pp. 132–145, 2015.

[12] M. Shahbazi et al., "Robotics-assisted mirror rehabilitation therapy: A therapist-in-the-loop assist-as-needed architecture," *IEEE/ASME Transactions on Mechatronics*, vol. 21, pp. 1954–1965, 2016.

[13] M. Sharifi et al., "Impedance learning-based adaptive control for human-robot interaction," *IEEE Transactions on Control Systems Technology*, pp. 1–14, 2021.

[14] J. Vantilt et al., "Model-based control for exoskeletons with series elastic actuators evaluated on sit-to-stand movements," *Journal of NeuroEngineering and Rehabilitation*, vol. 16, p. 65 (21 pages), 2019.

[15] A. Riani et al., "Adaptive integral terminal sliding mode control for upper-limb rehabilitation exoskeleton," *Control Engineering Practice*, vol. 75, pp. 108–117, 2018.

[16] R. Lu et al., "Development and learning control of a human limb with a rehabilitation exoskeleton," *IEEE Transactions on Industrial Electronics*, vol. 61, no. 7, pp. 3776–3785, 2014.

[17] M. Sharifi et al., "Assist-as-needed policy for movement therapy using telerobotics-mediated therapist supervision," *Control Engineering Practice*, vol. 101, p. 104481, 2020.

[18] A. Ijspeert et al., "From swimming to walking with a salamander robot driven by a spinal cord model," *Science*, vol. 315, pp. 1416–1420, 2007.

[19] S. Schrade et al., "Bio-inspired control of joint torque and knee stiffness in a robotic lower limb exoskeleton using a central pattern generator," in *International Conference on Rehabilitation Robotics (ICORR)*, 2017, pp. 1387–1394.

[20] K. Gui et al., "A generalized framework to achieve coordinated admittance control for multi-joint lower limb robotic exoskeleton," in *International Conference on Rehabilitation Robotics (ICORR)*, 2017, pp. 228–233.

[21] D. Zhang et al., "Cooperative control for a hybrid rehabilitation system combining functional electrical stimulation and robotic exoskeleton," *Frontiers in Neuroscience*, vol. 11, p. 725, 2017.

[22] J. K. Mehr et al., "Intelligent locomotion planning with enhanced postural stability for lower-limb exoskeletons," *IEEE Robotics and Automation Letters*, vol. 6, no. 4, pp. 7588–7595, 2021.

[23] K. Gui et al., "A practical and adaptive method to achieve emg-based torque estimation for a robotic exoskeleton," *IEEE/ASME Transactions on Mechatronics*, vol. 24, pp. 483–494, 2019.

[24] X. Liu and Q. Wang, "Real-time locomotion mode recognition and assistive torque control for unilateral knee exoskeleton on different terrains," *IEEE/ASME Transactions on Mechatronics*, 2020.

[25] X. Wu et al., "Individualized gait pattern generation for sharing lower limb exoskeleton robot," *IEEE Transactions on Automation Science and Engineering*, vol. 15, pp. 1459–1470, 2018.

[26] I. Kang et al., "Real-time neural network-based gait phase estimation using a robotic hip exoskeleton," *IEEE Transactions on Medical Robotics and Bionics*, vol. 2, pp. 28–37, 2019.

[27] R. Gupta et al., "Continuous angular position estimation of human ankle during unconstrained locomotion," *Biomedical Signal Processing and Control*, vol. 60, p. 101968, 2020.

[28] H. Kouzbary et al., "Generating an adaptive and robust walking pattern for a prosthetic ankle-foot by utilizing a nonlinear autoregressive network with exogenous inputs," *IEEE Transactions on Neural Networks and Learning Systems*, pp. 1–9, 2021.

[29] E. Diaconescu, "The use of narx neural networks to predict chaotic time series," *Wseas Transactions on computer research*, vol. 3, pp. 182–191, 2008.

[30] L. Xin et al., "Omnidirectional mobile robot dynamic model identification by narx neural network and stability analysis using the aplf method," *Symmetry*, vol. 12, p. 1430, 2020.

[31] H. Xie et al., "Time series prediction based on narx neural networks: An advanced approach," in *International Conference on Machine Learning and Cybernetics*, 2009, pp. 1275–1279.

[32] L. Du et al., "Response characteristics prediction of surge protective device based on narx neural network," *IEEE Transactions on Electromagnetic Compatibility*, vol. 62, pp. 74–82, 2020.

[33] V. Azimi et al. Robust Adaptive Impedance Control of Prosthetic Legs for Transfemoral Amputees. [Online]. Available: http://embeddedlab.csuohio.edu/prosthetics/research/robust-adaptive.html